Probabilistic Seismic Demand Model and Seismic Fragility Analysis of NPP Equipment Subjected to High- and Low-Frequency Earthquakes

Article *in* Nuclear science and engineering: the journal of the American Nuclear Society · July 2021

DOI: 10.1080/00295639.2021.1920796

CITATION
1

READS
86

7 authors, including:

Thanh-Tuan Tran
Kunsan National University
33 PUBLICATIONS **114** CITATIONS
SEE PROFILE

Le Mai Trang
Quy Nhon University
2 PUBLICATIONS **1** CITATION
SEE PROFILE

Phu-Cuong Nguyen
Ho Chi Minh City Open University
67 PUBLICATIONS **388** CITATIONS
SEE PROFILE

Doo Kie Kim
Kongju National University
166 PUBLICATIONS **1,252** CITATIONS
SEE PROFILE

Nuclear Science and Engineering

ISSN: (Print) (Online) Journal homepage: https://www.tandfonline.com/loi/unse20

Probabilistic Seismic Demand Model and Seismic Fragility Analysis of NPP Equipment Subjected to High- and Low-Frequency Earthquakes

Thanh-Tuan Tran, Thi-Mai-Trang Le, Phu-Cuong Nguyen, Dookie Kim, Thong M. Pham, Kashif Salman & Seongkyu Chang

To cite this article: Thanh-Tuan Tran, Thi-Mai-Trang Le, Phu-Cuong Nguyen, Dookie Kim, Thong M. Pham, Kashif Salman & Seongkyu Chang (2021): Probabilistic Seismic Demand Model and Seismic Fragility Analysis of NPP Equipment Subjected to High- and Low-Frequency Earthquakes, Nuclear Science and Engineering, DOI: 10.1080/00295639.2021.1920796

To link to this article: https://doi.org/10.1080/00295639.2021.1920796

Published online: 09 Jul 2021.

NUCLEAR SCIENCE AND ENGINEERING

DOI: https://doi.org/10.1080/00295639.2021.1920796

Probabilistic Seismic Demand Model and Seismic Fragility Analysis of NPP Equipment Subjected to High- and Low-Frequency Earthquakes

Thanh-Tuan Tran,[a,b] Thi-Mai-Trang Le,[b] Phu-Cuong Nguyen,[c] Dookie Kim,[d] Thong M. Pham,[e] Kashif Salman,[f] and Seongkyu Chang[g]*

[a]*Kunsan National University, Institute of Offshore Wind Energy, Jeollabuk-do, Korea*
[b]*Quy Nhon University, Faculty of Technology and Technique, Binh Dinh, Vietnam*
[c]*Ho Chi Minh City Open University, Faculty of Civil Engineering, Ho Chi Minh City, Vietnam*
[d]*Kongju National University, Department of Civil and Environmental Engineering, Chungcheongnam-do, Korea*
[e]*Curtin University, School of Civil and Mechanical Engineering, Bentley, Australia*
[f]*Innose Tech Company, Incheon, Korea*
[g]*Gwangju University, Department of Civil Engineering, Gwangju, Korea*

Received March 8, 2020
Accepted for Publication April 15, 2021

Abstract — *This study presents the Probabilistic Seismic Demand Model (PSDM) and explores optimal intensity measures (IMs) for nuclear power plant (NPP) equipment when subjected to ground motions having high-frequency (HF) and low-frequency (LF) contents. To this end, the PSDM is first constructed in terms of the IM and the corresponding engineering demand parameter, and its outcomes are utilized to select the optimum IMs based on the satisfaction of certain essential properties (i.e., efficiency, practicality, and proficiency). Regarding earthquake excitation, different IMs (i.e., structure-independent and structure-dependent IMs) are studied. The results show that the most appropriate IMs for the seismic performance of the cabinet are velocity spectrum intensity and spectral accelerations for the structure-independent IMs and the structure-dependent IMs, respectively.*

Moreover, fragility analysis is performed to assess the vulnerability of NPP equipment. The outcomes indicate that the cabinet is highly vulnerable to HF earthquakes as a consequence of response amplification. In addition, the selection of the earthquake IM has an important influence on the collapse capacity of the cabinet, and the fragility curves obtained from structure-dependent IMs are more reliable in comparison to those of structure-independent IMs.

Keywords — *Cabinet facility, cloud analysis, Probabilistic Seismic Demand Model, structural demand measure, optimal intensity measure.*

Note — *Some figures may be in color only in the electronic version.*

I. INTRODUCTION

Electrical cabinets are one of the pieces of critical equipment that is widely used in the nuclear industry.[1–3] The failure or collapse of one cabinet can lead to the failure of the entire electrical power system in a nuclear power plant[4–7] (NPP). Therefore, seismic performance evaluation of electrical cabinets has emerged as a major concern for safety-related NPP components. To date, many researchers have studied seismic risk assessment emphasizing cabinet vulnerability.[5,6,8–14] For example, Cao et al.[9] proposed a simplified approach to evaluate the capacity of the cabinet in relation to earthquakes. In this approach the cumulative absolute velocity is used as

*E-mail: skchang@gwangju.ac.kr

a ground motion intensity measure (IM). Later, Salman et al.[5] and Tran et al.[10] studied collapse risk assessment of cabinets, and average spectral acceleration $S_{\bar{a}}$ was chosen as an earthquake IM for seismic fragility analysis. However, current studies have not covered all the possible scenarios of the combination of nonstructural characteristics and earthquake IMs, which are classified into two categories: structure-independent IMs and structure-dependent IMs.

In the context of performance-based earthquake engineering, the Probabilistic Seismic Demand Model (PSDM) is the effective model to express the probability of a structural system under a given hazard environment.[15–17] Shome et al.[18] have proposed the PSDM, which builds the relationship between the structural demand measure (DM) and the earthquake IM. The PSDM is usually developed via linear regression analysis,[19,20] the outcomes of which can be used to select optimum IMs or determine the probability of collapse of structures. In the seismic evaluation, the optimal IMs can yield a close response prediction and reduce the deviation of the seismic performance of the structure. Selection of optimal IMs has been figured out in many works for different structures such as buildings,[21] bridges,[22] dams,[23] and so on. However, there is a limitation with NPP equipment.

Cabinet facilities are known as sensitive nonstructural components due to the resonance effects of the attacking of inside devices, and they often have higher dominant natural frequencies.[5,9,10] During earthquakes, the motion can be amplified if they have dominant high-frequency[24] (HF) pulses. Hence, the safety of these systems against high earthquake frequency contents is required. However, to date, understanding the dynamic behavior of cabinet facilities due to the earthquake frequency contents is very limited.

Based on the above discussion, the main objective of this study is to bridge the gaps in the seismic evaluation process for electrical cabinets in NPPs. The main contributions can be summarized as follows:

1. development of PSDMs of a cabinet for different IMs, i.e., structure-independent and structure-dependent IMs
2. selection of the optimal IM for the seismic performance of a cabinet based on the satisfaction of its essential qualities
3. seismic performance evaluation of an electrical cabinet considering the influence of the earthquake frequency contents.

II. PROTOTYPE AND FINITE ELEMENT MODEL OF CABINET

II.A. Cabinet Descriptions

In this study, a cabinet prototype provided by the Innose Tech Company (Korea) is utilized as a case study (Fig. 1a). The dimensions of the cabinet are 800-mm width (X), 800-mm depth (Y), and 2100-mm

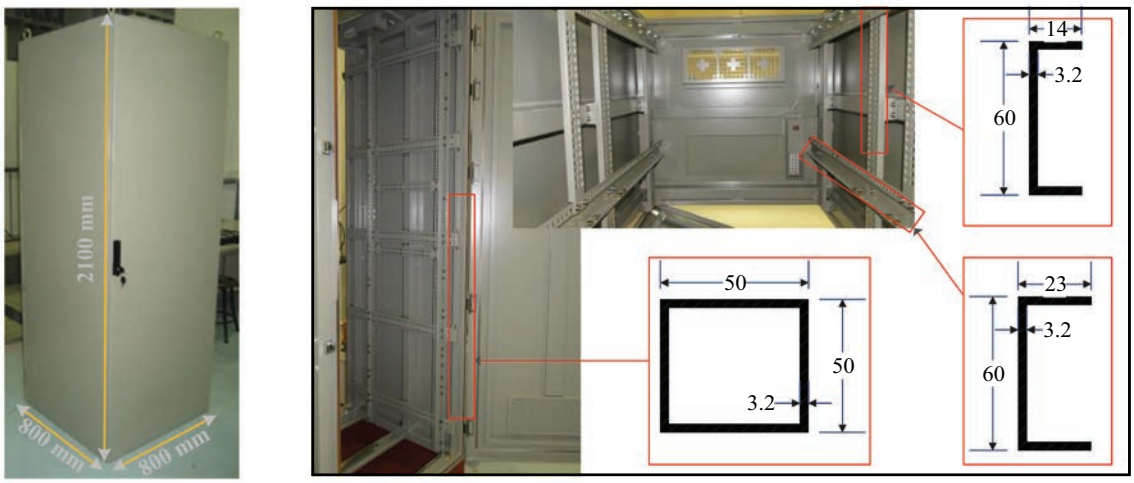

(a) (b)

Fig. 1. Configuration of the cabinet (in units of millimeter).

height (Z). The total weight of the cabinet is approximately 287 kg, and the weight of the door is 43.6 kg. The prototype is assembled by frame and plate members. The major sections of the main frame and subframe are rectangular and C-shaped, respectively, as shown in Fig. 1b. The screw connections are used to fix the frame and plate members together, and the hinge and the shim connections are used to join the door to the main frames. SS400 steel material with an elastic modulus of 200 GPa, density ρ of 7850 kg/m^3, and Poisson's ratio ν of 0.3 is used. The cabinet is anchored to the floor via C-shaped frames.

II.B. Nonlinear Modeling of Cabinet

The steel panels were attached to the frame members via welding or screws. These connectors are the significant elements for transferring the load from one member to another.[25,26] If the screw connectors are utilized, these fasteners may not be fully rigid.[4] During an earthquake, the failure modes of these connections can occur due to shear, tension, or a combination of both actions. The failure modes depend on the stiffness of the connection, which is a function of the thickness of the plates, the hole size, and the material strength.[27] In practice, it is difficult to determine the stiffness (force-deformation relationship) of screw connections; thus, the link element with the bilinear model is assumed, as shown in Fig. 2a. For each fastener, the shear force V_{AISI} and tensile force T_{AISI} are calculated using Eqs. (1) and (2) (Refs. 27,28, and 29):

$$V_{AISI} = \min\left(4.2\sqrt{t^3 d}F_u, 2.7tdF_u\right) \quad (1)$$

and

$$T_{AISI} = 0.85tdF_u \quad , \quad (2)$$

where

F_u = tensile strength
d = nominal diameter of screws
t = thickness of connected members.

In this study, the force-deformation relationships of the screw connection are taken from Hur.[4] The yielding forces are 12.46 and 4 kN for shear and tension, respectively, and the yield displacement limits are 0.3 cm.

Based on the above information, the finite element model (FEM) of the cabinet is developed using SAP2000 (Fig. 2b). In this model, beam and shell elements are assigned to the frame and plate members, respectively. Meanwhile, the connections between the frames and plates are simulated by zero-length elements, which can consider the stiffness properties of screw fasteners. For support boundary conditions, the fully fixed connections are assigned at the base of the model. In addition, the hinges are considered as the links between the doors and frames with five fixed degrees of freedom except for the rotation, and the locks are fixed at three translational degrees of freedom.

II.C. Validation of the Numerical Model

For validation, vibration tests with an impact hammer were performed.[30,31] Figure 3 shows the schematic of the overall test setup using an impact force with accelerometers attached to critical points. The impact

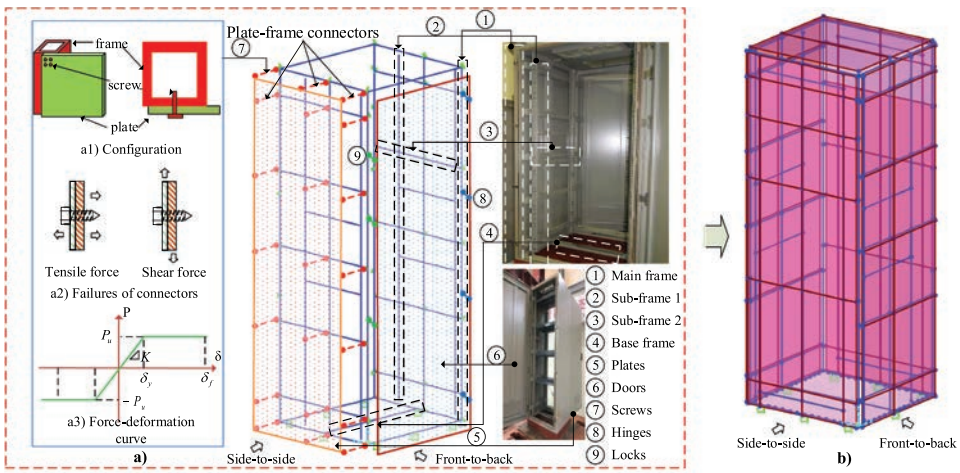

Fig. 2. Detailed descriptions of the numerical model.

force was excited at the top of the cabinet as shown in Fig. 3a. The maximum values of the impact force are 323 and 314 N for the front-to-back (FB) and side-to-side (SS) directions, respectively. Three accelerometers were distributed along the height of the cabinet, as shown in Fig. 3b. Both the input and output signals were recorded in the time domain, and they were used for experimental modal analysis.

The observed responses from the numerical analysis are compared with the experimental outcomes. The acceleration response and the corresponding response spectra at the top of the cabinet in both directions are presented in Figs. 4 and 5, respectively. As seen in Figs. 4 and 5, the FEM results make a good agreement with the experimental tests, although there was a minor difference in the FB direction. This variation can be attributed to the effects of hinge and shim connections:

1. In the real configuration, the doors are connected with main frames via hinge connectors. Thus,

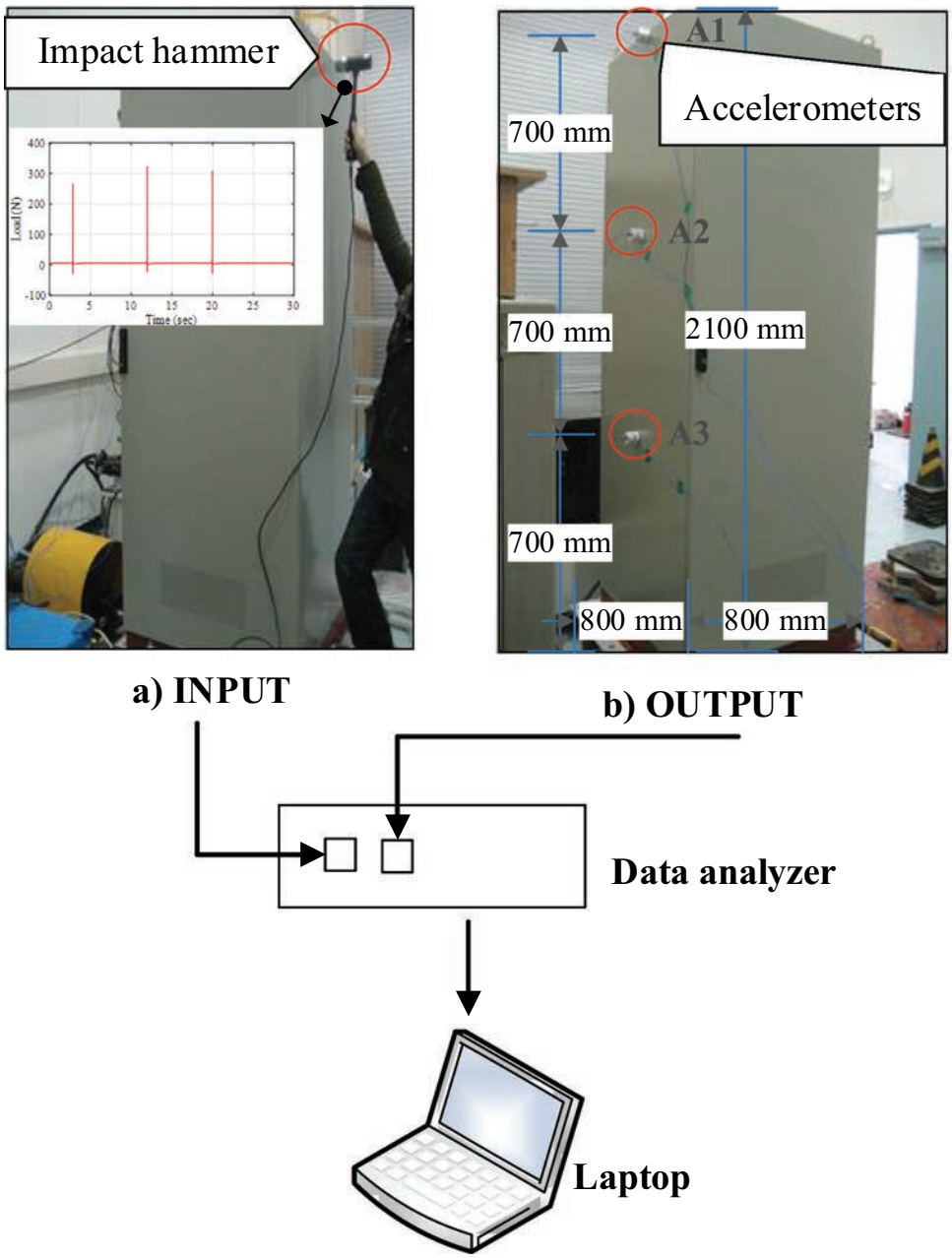

Fig. 3. Schematic of impact hammer test.

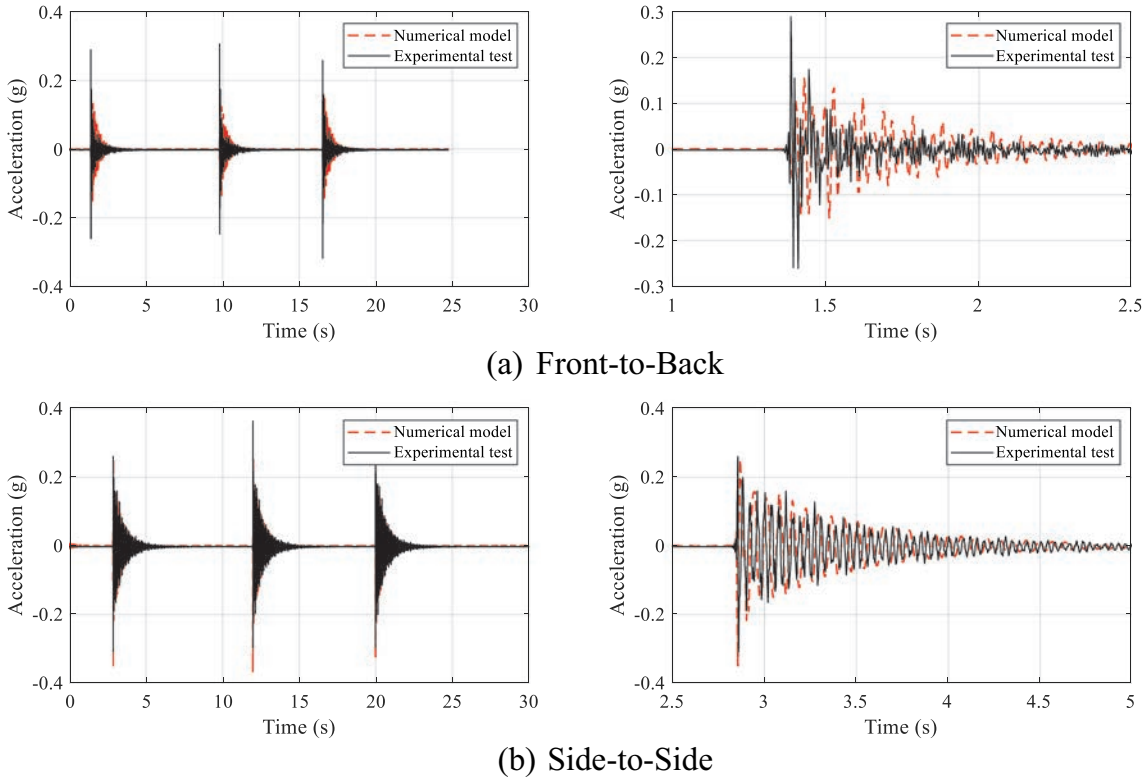

Fig. 4. Acceleration response at the top of the cabinet.

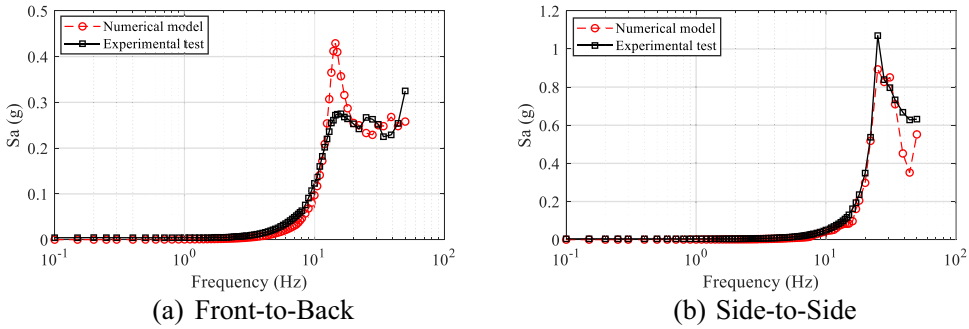

Fig. 5. Spectral acceleration response at the top of the cabinet.

the response is quite sensitive to their connections. During the impact tests, translations in three directions may occur; hence, the dynamic behavior of the equipment can be different from the numerical model.

2. The same phenomenon for the lock connectors may happen for the rotational degrees of freedom. Therefore, evaluation of the dynamic characteristics of the FEM should consider their modal sensitivity to their connections.

The responses from all accelerometers are measured and analyzed using the frequency domain decomposition method, which is a technique to identify the dynamic characteristics of a structure given multiple output data.[32] The first singular values of the power density matrix are reported, where the amplitudes are displayed against frequencies, as shown in Fig. 6. Based on Fig. 6, the fundamental natural frequencies of the electric cabinet in the FB and SS directions can be determined. Particularly, each frequency is represented by each

peak from the graph, and their values are tabulated in Table 1.

Through the numerical modal analysis, the natural frequencies from the FEM are evaluated. The differences in natural frequency values from the experiment and FEM results are expressed as follows:

$$rel.dif. = \frac{|f_{num} - f_{exp}|}{\left(\frac{f_{num}+f_{exp}}{2}\right)} 100 \quad , \tag{3}$$

where f_{num} and f_{exp} are the natural frequencies from the numerical analysis and experimental tests, respectively. As reported in Table 1, the natural angular frequencies retrieved from the FEM and experimental outcomes exhibit minor variations (less than 3.1%) in both directions. Therefore, it can be concluded that the FEM can represent the prototype, and it can be used for further investigations.

II.D. Limitation

In the current study, the numerical model of the cabinet is developed and verified with several assumptions. First, it is assumed to be fixed at the base. Second, only modal testing via the impact hammer test is performed; thus, the cabinet would not exhibit nonlinear behavior under impact forces. Therefore, in order to get an accuracy model, the following issues should be carried out for future studies:

1. the effects of the bolt connections between the cabinet and the shaking table
2. the sensitivity of the shim and hinge connections between the doors and main frames
3. The cabinet should be calibrated and verified with the shaking table test.

III. CLOUD-BASED FRAGILITY ANALYSIS

III.A. Selection of Ground Motions and IMs

In this study, two suites of ground motions that contain a total of 80 records are chosen. The magnitudes range from 5.2 to 7.6, and the closest distance-to-ruptured region (denoted as R_{RUP}) varies up to 250 km. The data are classified into two groups based on their dominant frequencies, one having a low-frequency (LF)

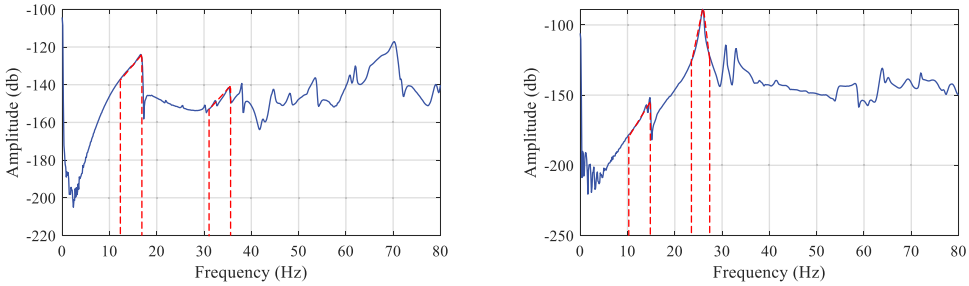

(c) Front-to-Back (d) Side-to-Side

Fig. 6. First singular vectors obtained from the numerical simulation.

TABLE 1

Natural Frequencies of the Electrical Cabinet*

Direction	Mode	Test	FEM	Relative Difference (%)
Front-to-back	1	15.10	14.08	1.74
	2	35.12	31.02	3.10
Side-to-side	1	14.75	14.17	1.00
	2	25.76	28.98	2.94

*Natural frequencies are in units of hertz.

earthquake, i.e., less than 10 Hz, and another one having a HF earthquake, i.e., greater than 10 Hz (Ref. 33). The former group consists of data from the worldwide history ground motion,[34] whereas the latter group is selected from the database in Korea and North America (Korea Meteorological Administration).[35] The details of selected earthquakes are given in the Appendix in Tables A.I and A.II. The response spectral accelerations of these sets are displayed in Fig. 7. In Figs. 7a and 7b, the first natural frequency of the cabinet is representative of the vertical line. Note that the selected data are used as the input of horizontal excitations at the base of the numerical model.

To identify the optimal IMs for the cabinet, different IMs of earthquakes are considered. They are classified into two categories: structure-independent IMs and structure-dependent IMs, as shown in Table 2. The former is the IMs that are independent of structural characteristics. These considered IMs have pros and cons when applied to the NPP components. The guideline BNL-NUREG -52007, entitled "Seismic Fragility of Nuclear Power Plant Components (PHASE II)," [36] states that modal sensitivity is a significant characteristic of the electrical cabinet, especially when evaluating the seismic behavior of this structure. Thus, the structure-dependent scalar IMs are recommended to surmount these drawbacks.

III.B. Performance Criteria

As pointed out in Refs. 4, 6, and 10, the cabinet facility is evaluated as a frequency-sensitive component because of the attacking of inside devices. Previous studies indicate that the acceleration response is a critical engineering demand parameter (EDP) for these frequency-sensitive components.[6,36–38] Therefore, in this study, this indicator is considered to be an EDP for evaluating the seismic response.

The limit state (LS) is one of the important requirements in the fragility analysis. The LS for a sensitive cabinet is defined based on BNL-NUREG-52007 (Ref. 36). This is conducted by the U.S. Nuclear Regulatory Commission, which is used to estimate the probabilistic fragility levels of electrical NPP equipment. In this research, the damage state is determined when the zero-period acceleration reaches 1.8 g.

III.C. Cloud Analysis

In the cloud analysis, a set of ground motion, which can be either scaled or unscaled data, is applied.[39,40] The ground motions are selected based on the objectives of the analysis. For each ground motion, a structure-specific engineering DM corresponding to the IM is obtained. The outcomes can be shown in either arithmetic or logarithmic ones.[19] Assuming that the ground motion IM expresses the lognormal distribution, the corresponding demand model can be calculated by following the exponential form[19]:

$$\mathrm{DM}(\mathrm{IM}) = A \cdot \mathrm{IM}^{B} \quad , \tag{4}$$

where A and B are the coefficients of the regression analysis. The parameters can be estimated by using the linear regression analysis. Thus, Eq. (4) is rewritten by the equivalent form of logarithms of the IM and DM as follows:

$$\ln(\mathrm{DM}(\mathrm{IM})) = A + B\ln(\mathrm{IM}) \quad . \tag{5}$$

Based on the cloud analysis results, the PSDM (also known as a fragility function) is derived.[10,41] The demand model is described as a straight line from a log-log plot of the IM-DM relationship with the dispersion of $\beta_{\mathrm{DM|IM}}$, and it is expressed as follows:

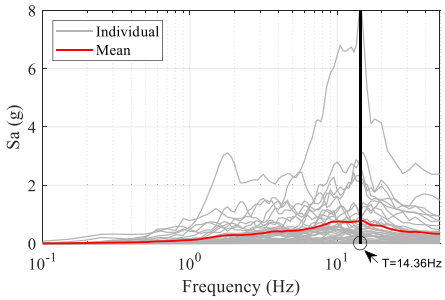

(a) High-frequency earthquakes

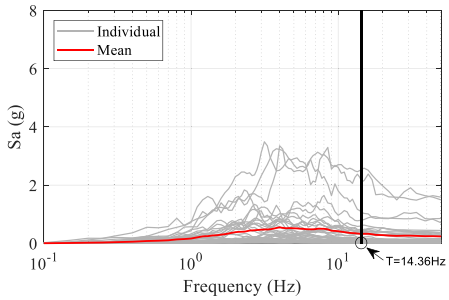

(b) Low-frequency earthquakes

Fig. 7. Response spectra of selected ground motions.

TABLE 2

Considered IMs

Category	Parameter	Definition	Reference
Structure-independent IMs	Peak values	$\mathrm{PGA} = \max(\lvert u(t)\rvert)(g)$ $\mathrm{PGV} = \max(\lvert \underline{u}(t)\rvert)(\mathrm{m/s})$ $\mathrm{PGD} = \max(\lvert u(t)\rvert)(\mathrm{m})$	
	Spectrum intensities	$\mathrm{ASI} = \int_{0.1}^{0.5} S_a(T, 5\%)dT(\mathrm{gs})$ $\mathrm{VSI} = \int_{0.1}^{2.5} S_v(T, 5\%)dT(\mathrm{m})$ $\mathrm{DSI} = \int_{2.0}^{5.0} S_d(T, 5\%)dT(\mathrm{ms})$	Bradley[42]
Structure-dependent IMs	Spectral response at T_1	$S_a(T_1)(g)$ $S_v(T_1)(\mathrm{m/s})$ $S_d(T_1)(\mathrm{m})$	Shome et al.[18]
	Spectral response at 10 Hz	$S_a^{10}(s)$ $S_v^{10}(\mathrm{m/s})$ $S_d^{10}(\mathrm{m})$	
	Spectral response at the frequency range of interest	$S_a^{4-16}(g)$ $S_v^{4-16}(\mathrm{m/s})$ $S_d^{4-16}(\mathrm{m})$	U.S. Nuclear Regulatory Commission[36]

$$P[\mathrm{DM} \geq dm|\mathrm{IM}] = 1 - \Phi\left(\frac{\ln(dm) - \ln(\mathrm{DM}(\mathrm{IM}))}{\beta_{\mathrm{DM|IM}}}\right) , \quad (6)$$

where $\Phi(.)$ refers to the standard normal cumulative distribution function and $\beta_{\mathrm{DM|IM}}$ is the standard deviation of the DM at the given IM, describing the uncertainty. Parameter $\beta_{\mathrm{DM|IM}}$ is obtained as a logarithmic standard deviation of errors, which is expressed in Eq. (7):

$$\beta_{\mathrm{DM|IM}} = \sqrt{\sum_{i=1}^{N} (e_i)^2/(N-2)} , \quad (7)$$

where N denotes the total number of samples and e_i is the residual between the actual value and the value predicted by the linear model. An example of the PSDM in the logarithmic scale domain is illustrated in Fig. 8, and it indicates that the selection of an appropriate IM can have a significant impact, which is expressed by the dispersion of responses.

III.D. Selection of an Optimal IM

According to Tothong and Luco[16] and Padgett et al.,[17] the optimal IM is selected in terms of efficiency, practicality, proficiency, and sufficiency conditions, which are described as follows:

1. *Efficiency*: This criterion relates to the prediction of a DM based on the IM considered. An efficient IM reduces the variations of observed response for a given IM, and it is assessed by the dispersion $\beta_{\mathrm{DM|IM}}$ in Eq. (7). An efficient IM shows low dispersion in the seismic response of the structure.

2. *Practicality*: This criterion reflects whether there is any correlation between the DM and the IM on the structure. The practicality aspect is evaluated by the regression parameter B in Eq. (5). A higher value indicates a high practical IM.

3. *Proficiency*: This criterion is a composite measure of efficiency and practicality. This indicator is proposed by Padgett et al.,[17] and it is known as the primary factor in the selection procedure. A more proficient IM has a lower modified dispersion ζ, thereby indicating the lower uncertainty.[17] The proficient indicator is expressed from Eqs. (5) and (6) as follows:

$$P[\mathrm{DM} \geq dm|\mathrm{IM}] = \Phi\left(\frac{\ln(\mathrm{IM}) - \frac{\ln(dm)-A}{B}}{\frac{\beta_{\mathrm{DM|IM}}}{B}}\right), \quad \text{where } \zeta = \frac{\beta_{\mathrm{DM|IM}}}{B} . \quad (8)$$

4. *Sufficiency*: This criterion is known as a secondary indicator and is used as a viable measure of its appropriateness for the developed PSDMs. It relates to the concept of statistical independence. In probabilistic terms, it is defined as follows[16]:

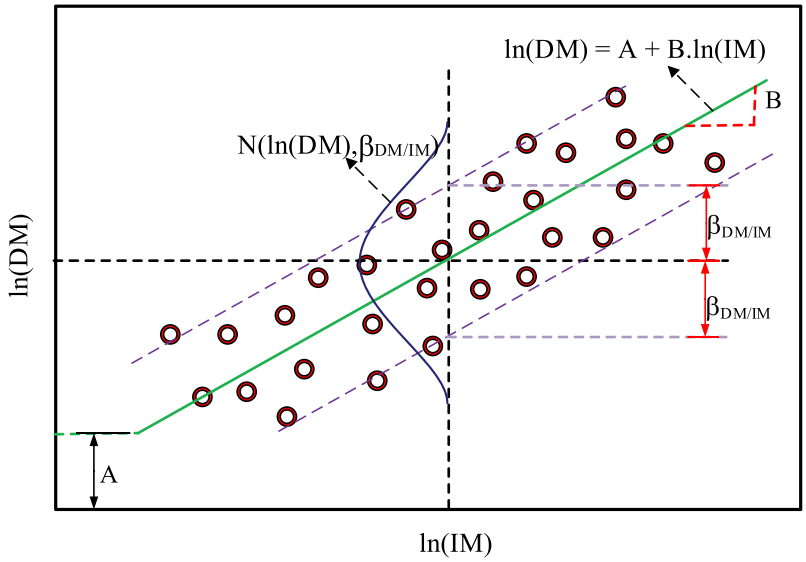

Fig. 8. Probabilistic seismic demand model.

$$P[\mathrm{DM} \geq dm|\mathrm{IM}] \cong P[\mathrm{DM} \geq dm|\mathrm{IM}, M, R] \quad , \qquad (9)$$

where M and R are the magnitude and the distance from the source to the site, respectively. The sufficiency is measured via the p-value, which is the probability of rejecting the null hypothesis. The p-value is calculated through performing a linear regression on the residuals, $\in^{\mathrm{EDP}}|\mathrm{IM}$, from the relationship of the PSDM and earthquake characteristics (i.e., M, R, and ε) (Ref. 23):

$$\in^{\mathrm{EDP}}|\mathrm{IM} = a_i + b_i(i) \quad , \qquad (10)$$

where a_i and b_i are the regression coefficients and i corresponds to the ground motion characteristics. In this study, because of the lack of ground motion characteristics, this indicator is not considered.

IV. RESULTS AND DISCUSSION

IV.A. Cloud Analysis

Figure 9 displays the results of cloud analysis for the cabinet using nonlinear time history analysis. The results are plotted in terms of peak ground acceleration (PGA) with acceleration response at the cabinet's top and illustrated either on the arithmetic or logarithmic scale. In each of Figs. 9a and 9b, two groups of scatter points are graphed: (1) the red points represent the HF earthquakes and (2) the blue points represent the LF earthquakes. To develop the PSDMs for the cabinet response, the linear regression analysis is performed on the logarithmic scale for all IMs. More details are presented in Sec. IV.B.

IV.B. Comparison of PSDMs and IMs

IV.B.1. PSDM Comparison

Figure 10 shows the PSDMs of the electrical cabinet in terms of the DM and the different IMs (Figs 10a through 10o are all in lognormal scale). The former is characterized by the acceleration response at the top of the electrical cabinet, and the latter is taken from Sec. III.A. Data regressions are separately done for two bins of ground motions, which are (1) red data points for HF earthquakes and (2) blue data points for LF earthquakes. In each of Figs 10a through 10o, the regression prediction lines of HF and LF ground motions, which are represented by the solid lines, are compared to each other. In particular, Figs. 10a through 10f show the comparison of the PSDMs of different structure-independent IMs. The results indicate that there is a distinct separation between the HF and the LF groups. The slopes of the regression lines from the HF earthquakes are smaller than those obtained from the LF earthquakes, with an average difference of 16%. However, using the structure-dependent IMs, the outcomes are crisper, especially for $S_a(T_1), S_v(T_1)$, and $S_d(T_1)$, as shown in Figs. 10j through 10m. Like the structure-independent IMs, the slopes of the regression lines observed from the structure-dependent IMs have the same trend for the HF and the LF groups, with an average difference of 2.8%. Moreover, the spectral acceleration responses $[S_a(10), S_a(T_1)$, and $S_a^{4-16}]$, having a slope in the range of 0.90 to 0.96, exhibit the most appropriate IMs in comparison with the others. The efficiency and practicality of these models are discussed in detail via the estimated parameters [Eqs. (5), (7), and (8)] in Sec. IV.B.2.

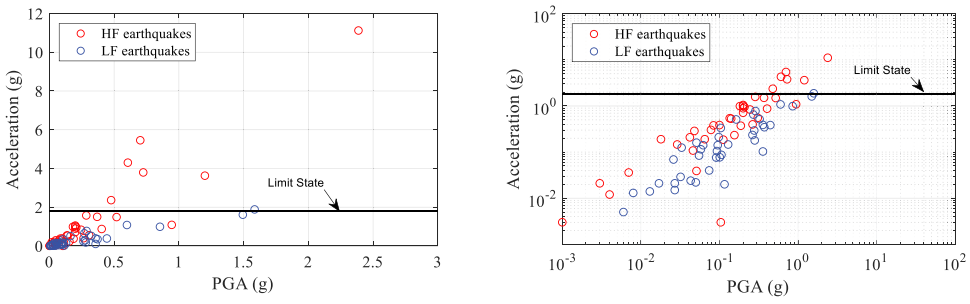

(a) Arithmetic scale (b) Logarithmic scale

Fig. 9. Cloud analysis results.

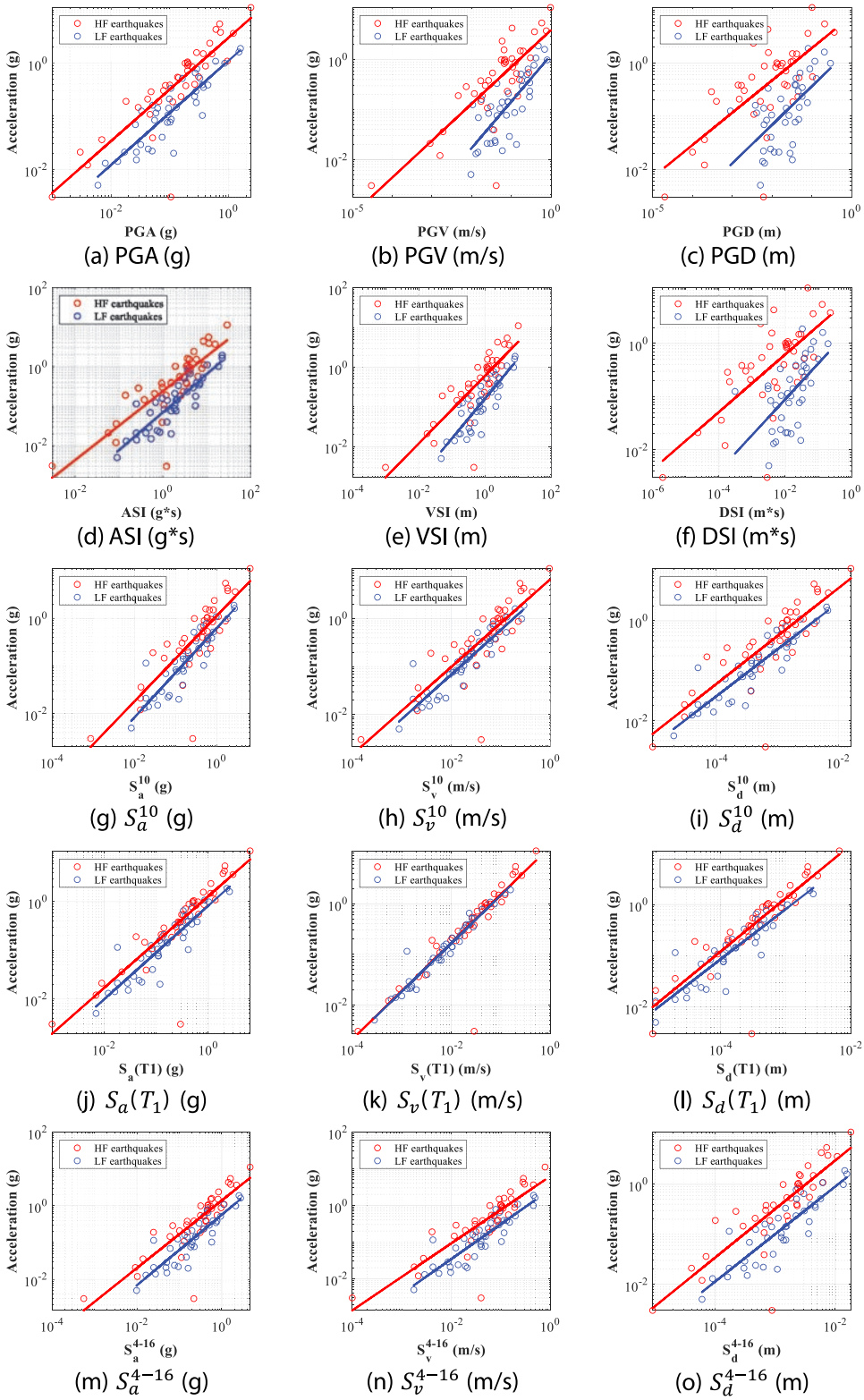

Fig. 10. PSDMs for different IMs.

IV.B.2. Intensity Measure Comparison

The optimality of an IM is evaluated based on the satisfaction of its essential qualities such as efficiency, practicality, and proficiency. It is worth mentioning that efficiency is the main parameter for the selection of the IM. The statistics of the estimated parameters of each

PSDM, i.e., values of intercept A, slope B, associated dispersion $\beta_{DM|IM}$, and correlation coefficient R, are enumerated in Table 3. Figures 11, 12, and 13 help in comparing the optimality between IMs. The main findings are as follows:

1. *Efficiency*: The efficiency of different IMs is displayed in Fig. 11. For structure-independent IMs (Fig. 11a), the peak values [PGA, peak ground velocity (PGV), peak ground displacement (PGD)] are found to exhibit an identical trend, while the spectrum intensities are more efficient, implying the lower dispersions [except for acceleration spectrum intensity (ASI) of HF earthquakes]. For instance, the dispersion values of the velocity spectrum intensity (VSI) are 0.24 and 0.13, resulting in 73% and 84% reductions for HF and LF, respectively, in comparison with PGV. For structure-dependent IMs (Fig. 11b), the spectral accelerations [$S_a(10)$, $S_a(T_1)$, andS_a^{4-16}] tend to be the most efficient IMs. The observed values of $S_a(T_1)$ and S_a^{4-16} for HF earthquakes are the same, with a value of 0.81; however, they are 0.73 and 0.58 for LF ground motions. These results indicate that the higher the number of modes is, the higher is the efficiency in the seismic response.

2. *Practicality*: The values of coefficient B in Fig. 12 indicate that the slope of the linear regression is nearly identical for all IMs. In the case of structure-independent IMs, the practicality of the LF group is slightly higher than that observed from the HF group,

TABLE 3

Statistics of the Estimated Parameters of Demand Models*

Intensity Measure	A		B		$\beta_{DM\|IM}$		ζ		R	
	HF	LF	HF	LF	HF	LF	HF	LF	HF	LF
PGA	1.11	0.11	*0.98*	*0.98*	1.06	0.92	1.08	0.94	0.92	0.94
PGV	1.37	0.23	0.74	0.93	0.89	0.83	1.20	0.89	0.86	0.84
PGD	2.05	0.66	0.61	0.73	0.96	0.83	1.57	1.14	0.52	0.71
ASI	−1.41	−2.64	0.88	0.96	*0.21*	1.57	*0.24*	1.64	0.93	0.93
VSI	−0.50	−1.83	0.85	1.01	0.24	*0.13*	0.28	*0.13*	0.93	0.93
DSI	2.02	0.69	0.54	0.67	0.83	0.79	1.54	1.18	0.15	0.65
S_a^{10}	0.12	−0.47	0.90	0.94	*0.68*	*0.61*	*0.76*	0.65	0.93	0.94
S_v^{10}	1.90	1.61	0.92	0.93	1.22	1.36	1.33	1.46	0.94	0.92
S_d^{10}	5.90	5.14	0.96	0.94	2.02	2.05	2.10	2.18	0.93	0.94
$S_a(T_1)$	0.26	−0.19	0.94	0.96	0.81	0.73	0.86	0.76	0.97	0.94
$S_v(T_1)$	2.61	2.59	0.95	0.95	1.41	1.62	1.48	1.71	0.97	0.98
$S_d(T_1)$	7.45	6.54	*1.04*	*0.98*	2.25	2.24	2.16	2.29	0.97	0.94
S_a^{4-16}	0.33	−0.57	0.92	0.96	0.81	0.58	0.88	*0.60*	0.96	0.93
S_v^{4-16}	1.84	1.01	0.92	0.95	1.19	1.20	1.29	1.26	0.94	0.91
S_d^{4-16}	5.57	4.28	0.97	0.95	1.98	1.93	2.04	2.03	0.93	0.91

*Values in italic type indicate most practical B, efficient $\beta_{DM|IM}$, or proficient ζ.

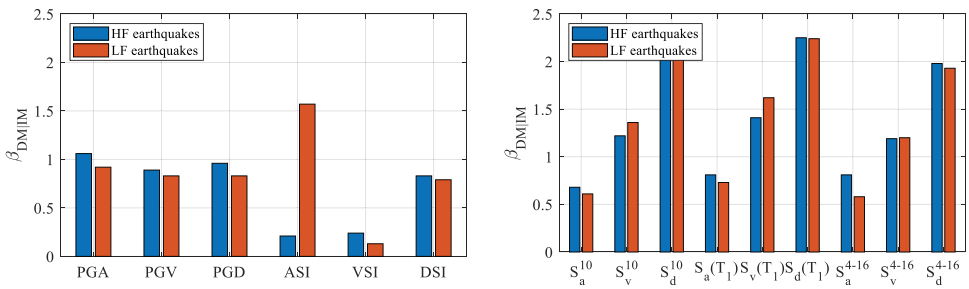

(a) Structure-independent IMs (b) Structure-dependent IMs

Fig. 11. Comparison of IM efficiency.

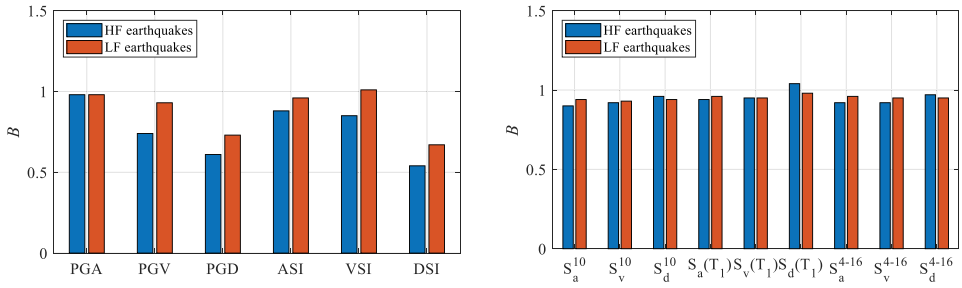

(a) Structure-independent IMs (b) Structure-dependent IMs

Fig. 12. Comparison of IM practicality.

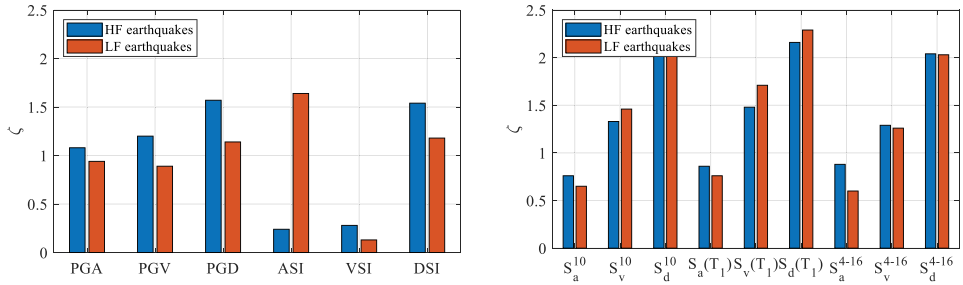

(a) Structure-independent IMs (b) Structure-dependent IMs

Fig. 13. Comparison of IM proficiency.

the average value being 15%. This indicates that the practical feature of the LF earthquakes is higher than HF earthquakes. In the case of structure-dependent IMs, the results show that all IMs have identical practicality for two suites of earthquakes; the ratio of two bins of earthquakes is nearly constant, which is approximately 1. This means that all structure-independent IMs have the same impact on the practicality of PSDMs.

3. *Proficiency*: The proficient indicator ζ for the two groups is shown in Fig. 13. In the case of structure-independent IMs, the values of the HF earthquakes are slightly greater than the LF earthquakes; the ratios of two bins of earthquakes range from 1.15 to 1.38. Notably, for ASI, the proficient value of the LF earthquakes is 0.24, which is smaller than about seven times in comparison with the HF earthquakes, while in structure-dependent IMs, the lowest modified dispersions are found for $S_a(T_1)$ and S_a^{4-16} and the largest modified dispersion is observed for $S_d(T_1)$ and S_d^{4-16}, which are the same trends with the efficient indicator. This can be explained as follows: The modified dispersion is proportional to the efficient indicator $\beta_{DM|IM}$, and since $\beta_{DM|IM}$ increases, the corresponding value of ζ increases.

IV.C. Cloud-Based Fragility Analyses

The probability of exceeding is defined based on the PSDM given in Sec. IV.B. The fragility curves of the cabinet are constructed for different IMs of two sets of ground motions, as given in Fig. 14. As seen, the fragility curves of Figs. 14a through 14o show an identical trend to HF and LF earthquakes. Particularly, the fragility curves under the HF earthquakes are higher sensitivity than the LF earthquakes. This means that the seismic vulnerability to the HF earthquakes tends to be higher than the LF earthquakes. Another finding is that the fragility functions obtained from the structure-independent IMs show large gaps between HF and LF ground motions (Figs. 14a through 14f) whereas the fragility functions observed from the structure-dependent IMs exhibit smaller gaps (Figs. 14g through 14o), implying more reliability in the collapse evaluation of the structure. This observation reveals that the structure-independent IMs are more sensitive in comparison with the structure-dependent IMs.

Figures 15 and 16 compare fragility curves for two groups of IMs, structure-independent IMs and structure-dependent IMs, respectively. For a better comparison, the curves are normalized with the median values of the

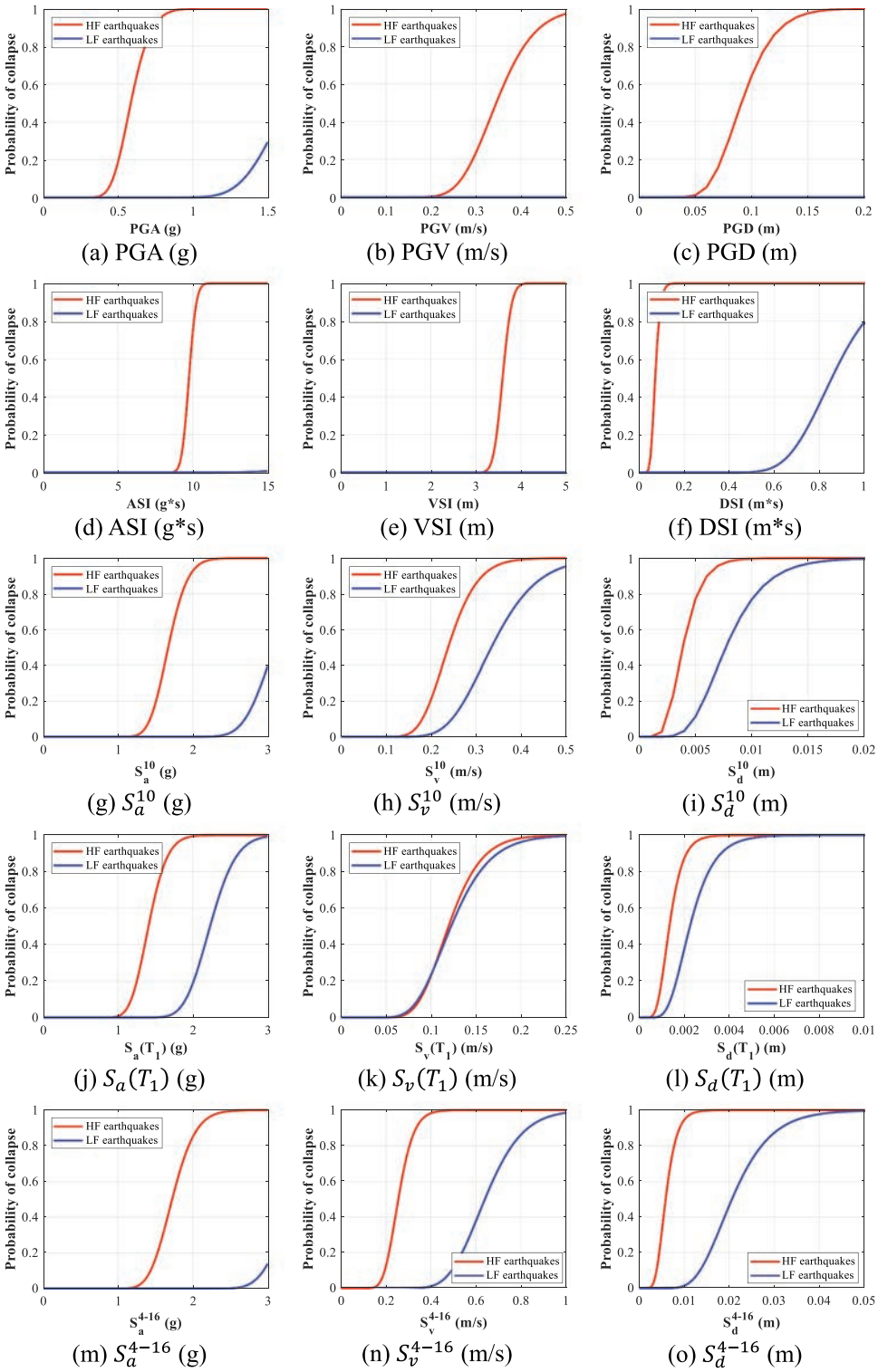

Fig. 14. Fragility curves for different IMs.

fragility function. As seen in Fig. 15, the fragility curves observed based on spectrum intensity are steeper than those obtained from peak values. This can be explained via their efficiencies shown in Fig. 11a. With regard to the structure-dependent IMs (Fig. 16), the higher efficiencies of spectral accelerations [i.e., $S_a(T_1), S_a(10),$ and $S_a(4-16)$] are found, leading to the steeper of the fragility curves in comparison with others.

V. CONCLUSIONS AND FUTURE WORK

This paper aims to identify the optimal IMs for seismic assessment of NPP equipment in terms of the satisfaction of certain essential properties. Different IMs, i.e., structure-independent IMs and structure-dependent IMs, are considered. Additionally, the uncertainties in seismic characteristics are investigated against two suites of ground motions, including HF and LF earthquakes. Based on the obtained results, the main findings can be drawn as follows:

1. Among the structure-independent IMs, the spectrum intensities are more efficient in comparison with peak values (PGA, PGV, and PGD). For instance, the use of VSI as the IM results in 73% and 84% reductions in the dispersion for HF and LF, respectively, in comparison with PGV, whereas in the case of the structure-dependent IMs, the spectral accelerations $S_a(T_1), S_a^{10}$, and S_a^{4-16} are the most appropriate IMs.

2. Investigating the practicality of IMs, the results reveal that both structure-independent and structure-dependent IMs are found to be nearly identical for HF and LF ground motions. Thus, they have the same impact on the practicality of PSDMs.

3. Examining the proficiency of IMs, the results show that in the case of the structure-independent IMs, the use of VSI as the IM has the highest proficiency in comparison with other IMs. In contrast, the spectral acceleration responses become most proficient for the structure-dependent IMs.

Therefore, when evaluating the seismic vulnerability of the cabinet, the uses of VSI and spectral acceleration are recommended for structure-independent and structure-dependent IMs, respectively.

Moreover, the collapse capacity of the electric cabinet is also investigated by using the fragility curves developed from the PSDMs. The results show that the cabinet facility is highly vulnerable to HF earthquakes. Also, the selection of IMs has an important influence on the collapse capacity of the NPP equipment.

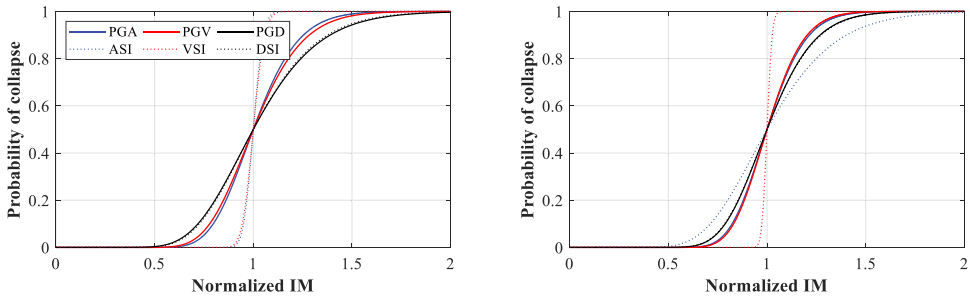

(a) High-frequency earthquakes (b) Low-frequency earthquakes

Fig. 15. Fragility curves based on structure-independent IMs.

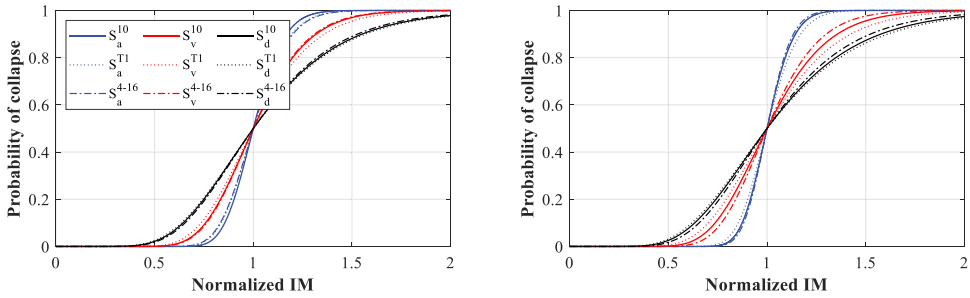

(a) High-frequency earthquakes (b) Low-frequency earthquakes

Fig. 16. Fragility curves based on structure-dependent IMs.

Particularly, the fragility curves obtained from structure-dependent IMs show a smaller gap between HF and LF earthquakes, indicating more reliability in comparison with structure-independent IMs.

APPENDIX

Details of selected earthquakes are given in Tables A.I and A.II.

TABLE A.I

High-Frequency Earthquakes

Record	Earthquake Name	Year	Magnitude	R_{RUP} (km)	$V_{s,30}$ (m/s)	PGA (g)
1	Helena_ Montana-02	1935	6	2.92	551.82	0.606
2	Imperial Valley-05	1955	5.4	14.88	213.44	0.477
3	Lytle Creek	1970	5.33	19.35	813.48	0.369
4	San Fernando	1971	6.61	130.98	591	0.135
5	San Fernando	1971	6.61	1.81	2016.13	0.084
6	San Fernando	1971	6.61	28.99	452.86	0.078
7	San Fernando	1971	6.61	24.87	389	0.285
8	Hollister-03	1974	5.14	10.46	1428.14	0.404
9	Hollister-03	1974	5.14	9.11	335.5	0.208
10	Friuli_ Italy-01	1976	6.5	49.38	496.46	0.245
11	Gazli_ USSR	1976	6.8	5.46	259.59	2.387
12	Imperial Valley-06	1979	6.53	0.34	259.86	0.2
13	Imperial Valley-06	1979	6.53	15.3	259.86	0.2
14	Imperial Valley-06	1979	6.53	21.68	237.33	0.2
15	Mammoth Lakes-06	1980	5.94	16.03	537.16	0.2
16	Nahanni_ Canada	1985	6.76	9.6	605.04	0.048
17	Nahanni_ Canada	1985	6.76	4.93	605.04	0.051
18	Nahanni_ Canada	1985	6.76	5.32	605.04	0.042
19	Landers	1992	7.28	2.19	1369	0.004
20	Northridge-01	1994	6.69	20.72	450.28	0.112
21	CA/Baja Border Area	2002	5.31	53.08	276.25	0.155
22	San Simeon_ CA	2003	6.52	212.98	420.48	0.1
23	San Simeon_ CA	2003	6.52	186.24	643.91	0.046
24	El Mayor-Cucapah, Mexico	2010	7.2	91.61	501	0.029
25	El Mayor-Cucapah_ Mexico	2010	7.2	239.03	388.68	0.702
26	Geonju	2016.9.12	5.4	5.86	SB[a]	0.307
27	Geonju	2016.9.12	5.4	8.23	SC[a]	0.187
28	Geonju	2016.9.12	5.4	22.15	SB	0.141
29	Pohang	2017.11.15	5.5	25.99	N/A[b]	0.945
30	Pohang	2017.11.15	5.5	22.69	N/A	1.201
31	Pohang	2017.11.15	5.5	9.46	N/A	0.519
32	Pohang	2017.11.15	5.5	28.04	N/A	0.182
33	N/A	2007	N/A	N/A	N/A	0.725
34	N/A	2007	N/A	N/A	N/A	0.003
35	N/A	2013	N/A	N/A	N/A	0.065
36	N/A	2014	N/A	N/A	N/A	0.018
37	N/A	2014	N/A	N/A	N/A	0.007
38	N/A	N/A	N/A	N/A	N/A	0.001
39	N/A	N/A	N/A	N/A	N/A	0.104
40	N/A	N/A	N/A	N/A	N/A	0.264

[a]SB, SC = soil classification according to Korean standard.
[b]N/A = not available.

TABLE A.II

Low-Frequency Earthquakes

Record	Earthquake Name	Year	Magnitude	R_{RUP} (km)	$V_{s,30}$ (m/s)	PGA (g)
1	Imperial Valley-02	1940	6.95	6.09	213.44	0.281
2	Parkfield	1966	6.19	9.58	289.56	0.444
3	Parkfield	1966	6.19	15.96	527.92	0.357
4	San Fernando	1971	6.61	110.18	441.25	0.008
5	San Fernando	1971	6.61	25.47	415.13	0.098
6	San Fernando	1971	6.61	21.5	969.07	0.095
7	San Fernando	1971	6.61	38.97	529.09	0.104
8	San Fernando	1971	6.61	205.77	354.06	0.027
9	San Fernando	1971	6.61	108.01	459.37	0.074
10	San Fernando	1971	6.61	124.79	442.88	0.006
11	San Fernando	1971	6.61	63.79	669.48	0.043
12	San Fernando	1971	6.61	124.41	322.42	0.013
13	San Fernando	1971	6.61	61.73	487.23	0.051
14	San Fernando	1971	6.61	70.23	347.67	0.017
15	San Fernando	1971	6.61	39.45	298.68	0.058
16	San Fernando	1971	6.61	62.23	486	0.026
17	Managua_ Nicaragua-01	1972	6.24	4.06	288.77	0.101
18	Managua_ Nicaragua-02	1972	5.2	4.98	288.77	0.055
19	Friuli_ Italy-01	1976	6.5	33.4	249.28	0.372
20	Friuli_ Italy-01	1976	6.5	80.41	352.05	0.263
21	Friuli_ Italy-01	1976	6.5	102.15	356.39	0.062
22	Friuli_ Italy-01	1976	6.5	15.82	505.23	0.05
23	Tabas_ Iran	1978	7.35	120.81	377.56	0.033
24	Tabas_ Iran	1978	7.35	28.79	324.57	0.357
25	Tabas_ Iran	1978	7.35	91.14	302.64	0.091
26	Tabas_ Iran	1978	7.35	194.55	280.26	0.106
27	Tabas_ Iran	1978	7.35	151.16	354.37	0.324
28	Tabas_ Iran	1978	7.35	2.05	766.77	0.093
29	Imperial Valley-06	1979	6.53	0.65	242.05	0.032
30	Imperial Valley-06	1979	6.53	10.42	208.71	0.027
31	Imperial Valley-06	1979	6.53	10.45	231.23	0.854
32	Imperial Valley-06	1979	6.53	24.6	205.78	0.287
33	Imperial Valley-06	1979	6.53	7.29	242.05	0.599
34	Imperial Valley-06	1979	6.53	50.1	336.49	0.163
35	Cape Mendocino	1992	7.01	6.96	567.78	0.277
36	Northridge-01	1994	6.69	7.01	2016.13	0.129
37	Kobe_ Japan	1995	6.9	0.96	312	0.27
38	Kobe_ Japan	1995	6.9	0.27	312	0.116
39	Kocaeli_ Turkey	1999	7.51	13.49	523	1.494
40	Chi-Chi_ Taiwan	1999	7.62	9.76	438.19	1.585

Acronyms

ASI: acceleration spectrum intensity
DM: demand measure
DSI: displacement spectrum intensity
EDP: engineering demand parameter
FB: front-to-back
FEM: finite element model
HF: high frequency
IM: intensity measure
LF: low frequency
LS: limit state
NPP: nuclear power plant
PGA: peak ground acceleration
PGD: peak ground displacement
PGV: peak ground velocity
PSDM: Probabilistic Seismic Demand Model
SS: side-to-side
VSI: velocity spectrum intensity

Nomenclature

B = practical factor
e_i = residual between the actual value and the predicted value
f_{exp} = natural frequencies from the experimental test
f_{num} = natural frequencies from the numerical model
M = magnitude
N = total number of samples
R = distance from the source to the site
$S_a(T_1)$ = spectral acceleration at T_1
$S_d(T_1)$ = spectral displacement at T_1
$S_v(T_1)$ = spectral velocity at T_1
S_a^{10} = spectral acceleration at T_{10}
S_d^{10} = spectral displacement at T_{10}
S_v^{10} = spectral velocity at T_{10}
S_a^{4-16} = spectral acceleration at the frequency range (4 to 16 Hz)
S_v^{4-16} = spectral velocity at the frequency range (4 to 16 Hz)
S_d^{4-16} = spectral displacement at the frequency range (4 to 16 Hz)

Greek

$\beta_{DM|IM}$ = standard deviation/efficiency factor
ζ = proficiency factor
$\Phi(.)$ = standard normal cumulative distribution function

Acknowledgments

This work was supported by the Korea Institute of Energy Technology Evaluation and Planning and the Ministry of Trade, Industry & Energy of Korea (number 20171510101960) and by Gwangju University (KR) [2020].

ORCID

Thanh-Tuan Tran http://orcid.org/0000-0002-9488-450X
Seongkyu Chang http://orcid.org/0000-0002-7573-9040

References

1. S. G. CHO, D. KIM, and S. CHAUDHARY, "A Simplified Model for Nonlinear Seismic Response Analysis of Equipment Cabinets in Nuclear Power Plants," *Nucl. Eng. Des.*, **241**, *8*, 2750 (2011); https://doi.org/10.1016/j.nucengdes.2011.06.026.
2. T.-T. TRAN and D. KIM, "Uncertainty Quantification for Nonlinear Seismic Analysis of Cabinet Facility in Nuclear Power Plants," *Nucl. Eng. Des.*, **355**, 110309 (2019); https://doi.org/10.1016/j.nucengdes.2019.110309.
3. M. J. LAROCCO, "Nuclear Power Plant Systems and Equipment," *Nucl. Sci. Eng.*, **50**, *4*, 405 (1973); https://doi.org/10.13182/nse73-a26582.
4. J. HUR, "Seismic Performance Evaluation of Switchboard Cabinets Using Nonlinear Numerical Models," Georgia Institute of Technology (2012).
5. K. SALMAN, T.-T. TRAN, and D. KIM, "Grouping Effect on the Seismic Response of Cabinet Facility Considering Primary-Secondary Structure Interaction," *Nucl. Eng. Technol.*, **52**, *6*, 1318 (2019); https://doi.org/10.1016/j.net.2019.11.024.
6. K. SALMAN, T.-T. TRAN, and D. KIM, "Seismic Capacity Evaluation of NPP Electrical Cabinet Facility Considering Grouping Effects," *J. Nucl. Sci. Technol.*, **57**, *7*, 1 (2020); https://doi.org/10.1080/00223131.2020.1724206.
7. B. J. GOODNO et al., "Effects of the January 2010 Haitian Earthquake on Selected Electrical Equipment," *Earthq. Spectra*, **27**, Suppl. 1, 251 (2011); https://doi.org/10.1193/1.3636415.
8. S. G. CHO, S. CHANG, and D. SUNG, "Application of Tuned Mass Damper to Mitigation of the Seismic Responses of Electrical Equipment in Nuclear Power Plants," *Energies*, **13**, *2*, 427 (2020); https://doi.org/10.3390/en13020427.
9. A. T. CAO et al., "Simplified Approach for Seismic Risk Assessment of Cabinet Facility in Nuclear Power Plants

Based on Cumulative Absolute Velocity," *Nucl. Technol.*, **206**, *5*, 743 (2020); https://doi.org/10.1080/00295450.2019.1696643.

10. T.-T. TRAN et al., "Fragility Assessment for Electric Cabinet in Nuclear Power Plant Using Response Surface Methodology," *Nucl. Eng. Technol.*, **51**, *3*, 894 (2019); https://doi.org/10.1016/j.net.2018.12.025.
11. "Reducing the Risks of Nonstructural Earthquake Damage —A Practical Guide," 4th ed., U.S. Department of Homeland Security, Federal Emergency Management Agency (2012).
12. D. E. PEPLOW et al., "Calculating Nuclear Power Plant Vulnerability Using Integrated Geometry and Event/Fault-Tree Models," *Nucl. Sci. Eng.*, **146**, *1*, 71 (2004); https://doi.org/10.13182/NSE04-A2394.
13. T.-T. TRAN et al., "Seismic Behavior of Steel Cabinets Considering Nonlinear Connections and Site-Response Effects," *Steel Compos. Struct.*, **36**, *1*, 17 (2020).
14. T.-T. TRAN et al., "Seismic Vulnerability of Cabinet Facility with Tuned Mass Dampers Subjected to High- and Low-Frequency Earthquakes," *Appl. Sci.*, **10**, *14*, 4850 (2020); https://doi.org/10.3390/app10144850.
15. J. ZHONG et al., "Optimal Intensity Measures in Probabilistic Seismic Demand Models of Cable-Stayed Bridges Subjected to Pulse-Like Ground Motions," *J. Bridge Eng.*, **24**, *2* (2019); https://doi.org/10.1061/(ASCE)BE.1943-5592.0001329.
16. P. TOTHONG and N. LUCO, "Probabilistic Seismic Demand Analysis Using Advanced Ground Motion Intensity Measures," *Earthq. Eng. Struct. Dyn.*, **36**, *13*, 1837 (2007); https://doi.org/10.1002/eqe.696.
17. J. E. PADGETT, B. G. NIELSON, and R. DESROCHES, "Selection of Optimal Intensity Measures in Probabilistic Seismic Demand Models of Highway Bridge Portfolios," *Earthq. Eng. Struct. Dyn.*, **37**, *5*, 711 (2008); https://doi.org/10.1002/eqe.782.
18. N. SHOME et al., "Earthquakes, Records, and Nonlinear Responses," *Earthq. Spectra*, **14**, *3*, 469 (1998); https://doi.org/10.1193/1.1586011.
19. A. CORNELL et al., "Probabilistic Basis for 2000 SAC Federal Emergency Management Agency Steel Moment Frame Guidelines," *J. Struct. Eng.*, **128**, *4* (2002).
20. J. ZHONG et al., "Probabilistic Seismic Demand and Capacity Models and Fragility Curves for Reticulated Structures Under Far-Field Ground Motions," *Thin-Walled Struct.*, **137**, 436 (2019); https://doi.org/10.1016/j.tws.2019.01.032.
21. M. AMIRI and M. YAKHCHALIAN, "Performance of Intensity Measures for Seismic Collapse Assessment of Structures with Vertical Mass Irregularity," *Structures*, **24**, 728 (2020); https://doi.org/10.1016/j.istruc.2020.01.038.
22. L. JIANG et al., "Optimal Seismic Intensity Measure Selection for Isolated Bridges Under Pulse-Like Ground Motions," *Adv. Civ. Eng.*, **2019** (2019); https://doi.org/10.1155/2019/3858457.
23. M. A. HARIRI-ARDEBILI and V. E. SAOUMA, "Probabilistic Seismic Demand Model and Optimal Intensity Measure for Concrete Dams," *Struct. Saf.*, **59**, 67 (2016); https://doi.org/10.1016/j.strusafe.2015.12.001.
24. A. GUPTA et al., "Current State of In-Cabinet Response Spectra for Seismic Qualification of Equipment in Nuclear Power Plants," *Nucl. Eng. Des.*, **343**, 269 (2019); https://doi.org/10.1016/j.nucengdes.2018.12.017.
25. P. C. NGUYEN and S. E. KIM, "A New Improved Fiber Plastic Hinge Method Accounting for Lateral-Torsional Buckling of 3D Steel Frames," *Thin-Walled Struct.*, **127**, 666 (2018); https://doi.org/10.1016/j.tws.2017.12.031.
26. J. HENRIQUES et al., "Structural Performance of Light Steel Framing Panels Using Screw Connections Subjected to Lateral Loading," *Thin-Walled Struct.*, **121**, 67 (2017); https://doi.org/10.1016/j.tws.2017.09.024.
27. AISI S200-12, "North American Standard for Cold-Formed Steel Framing – General Provisions, 2012 Edition," American Iron and Steel Institute, Washington, D.C. (2012).
28. R. M. FRANCKA, "Screw Connections Subject to Tension Pull-Out and Shear Forces," Masters Thesis, Missouri University of Science and Technology (2009).
29. T. PEKOZ, "Design of Cold-Formed Steel Screw Connections," *Proc.10th Int. Specialty Conf. Cold-Formed Steel Structures*, St. Louis, Missouri, October 23–24, 1990, p. 575 (1990).
30. S. Y. KHOO et al., "Feasibility Study of Performing Experimental Modal Analysis with Oblique Impact Testing Using Various Oblique Impact Directions," *Alexandria Eng. J.*, **59**, *1*, 457 (2020); https://doi.org/10.1016/j.aej.2020.01.014.
31. Y. WENG et al., "Experimental and Numerical Investigations on Heat Transfer of Reactor Internals Under Direct Injection," *Nucl. Sci. Eng.*, **190**, *1*, 93 (2018); https://doi.org/10.1080/00295639.2017.1417345.
32. R. BRINCKER, L. ZHANG, and P. ANDERSEN, "Modal Identification of Output-Only Systems Using Frequency Domain Decomposition," *Smart Mater. Struct.*, **10**, *3*, 441 (2001); https://doi.org/10.1088/0964-1726/10/3/303.
33. D. D. NGUYEN et al., "Identifying Significant Earthquake Intensity Measures for Evaluating Seismic Damage and Fragility of Nuclear Power Plant Structures," *Nucl. Eng. Technol.*, **52**, *1*, 192 (2019); https://doi.org/10.1016/j.net.2019.06.013.
34. T. D. ANCHETA et al., "PEER NGA-West2 Database : A Database of Ground Motions Recorded in Shallow Crustal Earthquakes in Active Tectonic Regions,"*Proc. 15th World Conf. Earthquake Engineering*, Lisbon, Portugal, September 24–28, 2012, p. 30013 (2012).

35. Korea Meteorological Administration database; https://web.kma.go.kr/eng/index.jsp (current as of Mar. 8, 2020).

36. K. K. BANDYOPADHYAY et al., "Seismic Fragility of Nuclear Power Plant Components (PHASE II)," NUREG/CR-4659, BNL-NUREG-52007, Brookhaven National Laboratory/U.S. Nuclear Regulatory Commission (1991).

37. T.-T. TRAN, T.-H. NGUYEN, and D. KIM, "Seismic Incidence on Base-Isolated Nuclear Power Plants Considering Uni- and Bi-Directional Ground Motions," *J. Struct. Integr. Maint.*, **3**, *2*, 86 (2018); https://doi.org/10.1080/24705314.2018.1461547.

38. "High Frequency Program: Application Guidance for Functional Confirmation and Fragility Evaluation," Electric Power Research Institute (2015).

39. F. JALAYER et al., "Bayesian Cloud Analysis: Efficient Structural Fragility Assessment Using Linear Regression," *Bull. Earthq. Eng.*, **13**, *4*, 1183 (2015); https://doi.org/10.1007/s10518-014-9692-z.

40. A. ALI et al., "Seismic Vulnerability of Offshore Wind Turbines to Pulse and Non-Pulse Records," *Earthq. Eng. Struct. Dyn.*, **49**, *1*, 24 (2020); https://doi.org/10.1002/eqe.3222.

41. Y. M. MAHMOUD et al., "Assessment of Progressive Collapse of Steel Structures Under Seismic Loads," *Alexandria Eng. J.*, **57**, *4*, 3825 (2018); https://doi.org/10.1016/j.aej.2018.02.004.

42. B. A. BRADLEY, "Empirical Equations for the Prediction of Displacement Spectrum Intensity and Its Correlation with Other Intensity Measures," *Soil Dyn. Earthq. Eng.*, **31**, *8*, 1182 (2011); https://doi.org/10.1016/j.soildyn.2011.04.007.